Nucleation kinetics in deionized charged colloidal model systems: A quantitative study by means of classical nucleation theory

Patrick Wette[1] and Hans Joachim Schöpe[2]
[1]*Institut für Materialphysik im Weltraum, Deutsches Zentrum für Luft- und Raumfahrt, Linder Höhe, 51170 Köln, Germany*
[2]*Institut für Physik, Johannes Gutenberg-University Mainz, Staudinger Weg 7, 55128 Mainz, Germany*
(Received 24 February 2007; published 21 May 2007)

We have studied the nucleation kinetics of charged colloidal model systems under salt free conditions crystallizing in bcc structure covering a wide range of particle number densities 18 $\mu m^{-3} \leq n \leq 66.3$ μm^{-3}. We employed direct video-microscopic observation of individual nucleation events to obtain time resolved nucleation rate densities. Polarization microscopy and static light scattering on the resulting solids in combination with Avrami theory is used to determine the steady state nucleation rate at high undercoolings. The final nucleation rate densities J from different methods are observed to be consistent with each other. By increasing the difference in the chemical potential between melt and crystal $\Delta\mu$ about one order of magnitude J increases from 10^9 $m^{-3}s^{-1}$ to 10^{17} $m^{-3}s^{-1}$ over approximately seven orders of magnitude. The data can be well analyzed and interpreted using classical nucleation theory (CNT) leading to a linearly increasing melt-crystal surface tension. Surprisingly, the reduced surface tension is about one order of magnitude larger compared to other system (metals; hard sphere colloids). The critical radius of the crystal nuclei is decreasing down to a very small value of 1.5 coordination shells. The determined kinetic prefactors are up to 10 orders of magnitude smaller than the prefactor calculated by CNT.

DOI: 10.1103/PhysRevE.75.051405 PACS number(s): 82.70.Dd, 81.10.−h, 64.60.Qb

I. INTRODUCTION

Classical nucleation theory (CNT)—developed from the start of the past century [1–3]—predicts an exponential dependence of homogeneous nucleation rate densities J on the free energy barrier for nucleus formation ΔG^*: $J=J_0 \exp(-\Delta G^*/k_BT)$. Here J_0 is a kinetic prefactor, k_BT is the thermal energy, and $\Delta G^*=(16\pi/3)\gamma^3(n\Delta\mu)^{-2}$, where γ is the surface tension between the metastable parent phase and the crystal phase and $\Delta\mu$ is the chemical potential difference between the two phases. This theory has found widespread applications ranging from liquid droplet formation from the vapor to crystallization from supersaturated solutions or undercooled melts [4].

Despite its appealing simplicity, tests of this theory remain extremely difficult. In atomic or molecular systems the crystallization process is quite often not isothermal and the crystal growth is not linear—dentritic growth is often observed. Also the interaction between atoms and molecules is not well defined. In colloidal model systems crystallization is isothermal due to the presence of the solvent acting as an efficient heat sink, the interaction is analytically tractable as well as experimentally tunable, and the crystallization process is accessible by optical experiments like light scattering or microscopy [5–9]. But even in model systems of spherical colloidal particles as well as in computer simulations there are still problems due to the exponential dependence on the ratio between barrier height and thermal energy. The difficulties arising are the same as in atomic or molecular systems. Close to the phase boundary homogeneous nucleation is a rare event and solidification is dominated by growth after heterogeneous nucleation either at the container walls or impurities in the bulk [10,11]. In the interesting region of large metastabilities, where both the capillarity approximation and the approximation of independent nucleation events are expected to break down, nucleation becomes either extremely fast or may interfere with a kinetic glass transition [5,6,12]. Nevertheless, in the past few years there was a burst of activities triggered by novel experimental designs [13–18] and by substantial progress in computer power and design of algorithms [19–24].

Most experimental progress has been made with hard sphere systems, addressing growth velocities [25], nucleation rate densities [9,25–29], or ripening behavior [30]. For charged spheres growth seems relatively well understood and may be accurately described above the melting concentration using a Wilson-Frenkel law [31] for reaction controlled growth [6,11,32,33]. Nucleation in weakly charged systems has been studied only occasionally [34–36] but also data on highly charged spheres with their long ranged repulsion are particularly rare [37–39].

To the knowledge of the authors, there is no systematic study dealing with the determination of the surface tension γ or the kinetic prefactor J_0 in highly charged colloidal systems. For the nucleation process γ is a key parameter, as according to CNT it determines the height of the energy barrier that a precritical nucleus must overcome in order to keep growing while minimizing the free energy. The kinetic prefactor is the key parameter for calculating absolute values of the nucleation rate density. In a recent Letter we presented the first systematic measurements of the concentration dependence of charged sphere nucleation in the salt free case, using static light scattering techniques [40]. In a further paper we used microscopic investigation methods in order to get access to nucleation rate densities in the salt-free state at low particle number density [41]. In this paper we combine these techniques, and are able to access nucleation rate densities over 6.5 orders of magnitude ranging from very rare events close to the phase boundary to nearly instantaneous solidification at large metastability. We again interpret our

data in terms of CNT, yielding estimates for the melt-crystal interfacial tension as well as for the kinetic prefactor. We analyze our data in three different ways leading to slightly different results. We find that, within the experimental scatter, the surface tensions increase approximately linearly as the difference in the chemical potential increases. The prefactors, on the other hand, show huge deviations. The calculated critical radii of the nuclei reduce down to 1.5 coordination shells which is unphysically small.

The paper is organized as follows. We first provide a short overview of classical nucleation theory, adapted to the diffusive properties of charged colloidal systems. After that we outline the various techniques employed for sample preparation and observation. Our results and evaluations are presented and discussed in Sec. IV. We conclude with discussion of unresolved issues and suggest possible approaches to solve these.

II. SHORT CNT OVERVIEW

Classical nucleation theory (CNT) states that crystallization kinetics is controlled by an exponential dependence on the ratio between some intrinsic energy scale, and the thermal energy k_BT. From this, the nucleation rate density J is given as [2,3]

$$J = J_0 \exp(-\Delta G^*/k_BT), \tag{1}$$

where for colloidal systems the nucleation barrier $\Delta G^* = 16\pi\gamma^3/3(n\Delta\mu)^2$ is determined by the macroscopic surface tension γ, the difference in chemical potential $\Delta\mu$ between the melt and the solid phase, which is a measure of the degree of undercooling of the system, and the particle number density n. J_0 is a kinetic prefactor and was proposed to look as follows [6,42]:

$$J_0 = An\frac{D_S^L}{l^2}, \tag{2}$$

where D_S^L is the long time self-diffusion coefficient, A is a dimensionless factor, and l a characteristic length scale approximated successfully by $l=d_{NN}\approx n^{-1/3}$.

In former publications the dimensionless factor A was set to one as a first approximation, and a possible dependence of this factor on suspension parameters was not considered [6,42]. If one completely evaluates the factor A within the framework of classical nucleation theory for colloidal systems (see the Appendix) one arrives at the following expression for the kinetic prefactor:

$$J_0 = 1.55 \times 10^{11} n^{4/3}\sqrt{\gamma}D_S^L, \tag{3}$$

which is a function of the particle number density, the surface tension, and the long time self-diffusion coefficient. The final result for the nucleation rate density then reads

$$J = 1.55 \times 10^{11} n^{4/3}\sqrt{\gamma}D_S^L \exp\left(-\frac{16\pi\gamma^3}{3k_BT(n\Delta\mu)^2}\right). \tag{4}$$

To evaluate Eq. (4) one needs to know the difference in the chemical potential $\Delta\mu$ as a function of the particle number density n. Therefore it is necessary to characterize the used charge colloidal model system very accurately in terms of phase behavior, interaction energy and crystal growth velocity before measuring nucleation rate densities.

III. EXPERIMENT

A. Sample conditioning

The methods are described in detail elsewhere [43,44] and are briefly summarized here. For our investigations we used highly charged polystyrene-poly-*n*-butylacrylamide copolymer particles which were a kind gift of BASF AG Ludwigshafen (PnBAPS68 Lot no. ZK2168/7387). The particles are interacting by long range electrostatic repulsion and the pair energy in monodisperse charged colloidal systems can be written on the mean field level as

$$V(r) = \frac{(Z^*e)^2}{4\pi\varepsilon_0\varepsilon_r}\left(\frac{\exp(\kappa a)}{1+\kappa a}\right)^2\frac{\exp(-\kappa r)}{r}, \tag{5}$$

with the screening parameter κ calculated from the salt concentration c via

$$\kappa^2 = \frac{e^2}{\varepsilon_0\varepsilon_r k_BT}(nZ^* + n_{\text{salt}}), \tag{6}$$

where $\varepsilon_0\varepsilon_r$ is the dielectric permittivity of the suspension, k_BT is the thermal energy, and $n_{\text{salt}}=2000N_Ac$ is the number density of background electrolyte with N_A being Avogadro's number. Z^* is the effective charge of the particle and a the particle radius. The particles used were carefully characterized in previous experiments [45]. These particular particles was selected for several reasons. The particles are quite small and have a low polydispersity [$2a=(68\pm3)$ nm from ultracentrifugation], facilitating scattering experiments at particle number densities up to $n\approx 66\ \mu\text{m}^{-3}$ without strong multiple scattering. The effective charge from elasticity measurements is $Z_G^*=331\pm3$.

Together this leads to a low lying freezing transition under salt free conditions of very narrow width at $n=(6.1\pm0.5)\ \mu\text{m}^{-3}$ as determined by microscopy [46]. This narrowness is essential for an accurate estimate of $\Delta\mu$ determined in measurements of the crystal growth velocity. The crystal structure is body centered cubic and no kinetic glass transition is observed in the used particle concentration range. Systematic investigations of the nucleation rate densities with low systematic and statistical errors were possible over roughly one order of magnitude in particle concentration.

Samples were conditioned in a closed system under inert gas atmosphere. The suspension was filtered using a 500 nm filter to remove bigger aggregates which could cause heterogeneous nucleation. A gas tight tubing connects several devices including a reservoir to add water or suspension, an ion exchange column filled with mixed bed ion exchange resin (Amberlite UP 604, Rohm & Haas, France) a conductivity experiment and optical cells to simultaneously perform static light scattering and video microscopy. During preparation the suspension is driven through the circuit by a peristaltic pump. It is kept in a shear molten state but readily crystal-

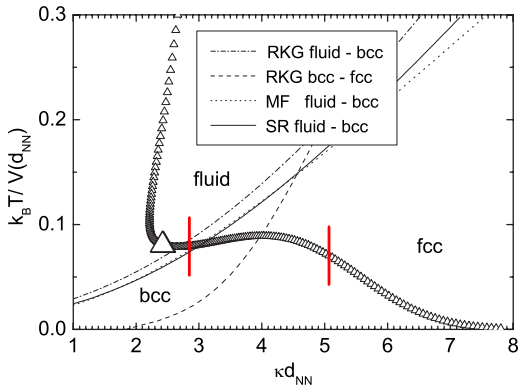

FIG. 1. (Color online) The universal phase diagram by Robins, Kremer, and Grest (RKG) [48], Mejer and Frenkel (MF) [50], and Stevens and Robbins (SR) [51] showing the reduced temperature–coupling strength plane. Symbols denote the pathway of our sample in this plane (up triangles) upon increasing the particle number density from 0.1 μm^{-3} (top) to 100 μm^{-3} (bottom right). These were calculated using the interaction determined in crystal elasticity measurements at a residual ion concentration of $c_s=2\times10^{-7}$ mol/l. The large triangle denotes the experimental freezing transition n_F. The two bars denotes the area of investigation ($n=18$ μm^{-3} to $n=66.3$ μm^{-3}).

lizes once shear is aborted. Completion of deionization is monitored via conductivity, typical residual ionic impurity concentrations are on the order of the ion product of water. The particle number density n is inferred from a combined Bragg scattering and conductivity experiment on the deionized sample [47].

Experiments were conducted at constant salt concentration $c_s=2\times10^{-7}$ mol l^{-1} and varying particle number density 18 $\mu m^{-3}\leq n\leq 66.3$ μm^{-3}. Each particular state prepared may be conveniently represented in terms of a point on a state line in a reduced temperature-coupling strength diagram, a phase diagram representation first suggested by Robbins, Kremer, and Grest [48,49]. Figure 1 shows this general path for PnBAPS68 under deionized conditions. The experimentally determined phase transition and the measurement range used to investigate crystal nucleation are also shown and can be compared to the predicted phase boundaries [48,50,51]. With increasing n the coupling parameter increases continuously, while the pair interaction energy, which is on the order of $15k_BT$, first decreases due to self-screening, then increases again due to the reduction of the interparticle separation.

B. Growth measurements

To obtain the difference in the chemical potential between melt and solid, $\Delta\mu$, and to determine the limiting growth velocity at large $\Delta\mu$, we performed extensive growth measurements. Since growth velocities are on the order of some $\mu m\ s^{-1}$, this is conveniently studied by Bragg microscopy. Details of those measurements are given elsewhere [11]. The velocity increases with increasing n to a limiting value of $v_\infty=(17.1\pm0.3)$ $\mu m\ s^{-1}$ and can be well described by a Wilson-Frenkel law: $v=v_\infty[1-\exp(-\Delta\mu/k_BT)]$, where we express $\Delta\mu$ in terms of a rescaled energy density: $\Delta\mu=B\Pi^*$ with $\Pi^*=(\Pi-\Pi_F)/\Pi_F$. Here the energy density $\Pi=\alpha nV(d_{NN})$ with α being the particle coordination number, $V(d_{NN})$ is the interaction energy at nearest neighbor distance, and F denotes freezing [11]. This approach considers both the direct density dependence of $\Delta\mu$ and the pair interaction potential $V(r)$. We obtain $B=1.64\pm0.20k_BT$.

C. Nucleation measurements

Three different techniques were employed in our nucleation measurements. At low n we used direct video microscopic imaging. At moderate to large n nucleation becomes too fast to be directly observed and we therefore determined the crystallite size distribution by microscopy and the average crystal size using static light scattering in combination with Avrami's theory [52]. All set ups are designed in that way that heterogeneous nucleated crystals at the container walls are excluded from the measured data. The use of these complementary methods with overlapping ranges of applicability allows us to determine nucleation rate densities over seven orders of magnitude. We give here only a short description of the direct microscopic methods and static light scattering, a detailed overview is given elsewhere [40,41].

1. *Video microscopy and polarization microscopy*

During conditioning the suspension is continuously cycled through the tubing system and kept in a shear molten state. Resolidification after abortion of shear is monitored in a flow through optical cell of rectangular cross section (1 mm×10 mm, Rank Bros. Bottisham Cambridge, UK). The cell was mounted on the stage of a polarization microscope equipped with a low resolution objective (Laborlux 12, Leitz, Wetzlar, D). Images are recorded by CCD-camera (EHD kampro04, 1/2 in. SVHS, EHD Physikalische Technik, D) and stored in a computer for later image analysis.

In polarization microscopy the sample is observed between two crossed polarizers. Colored crystallites appear on a nearly black background and grow in time. As the samples under investigation show a cubic crystal structure the contrast mechanism cannot rely on optical anisotropy. Instead dynamical diffraction theory may explain the observations [53,54]. As we are working with low magnification objectives the minimum detectable crystal size is about 5–10 μm, which is slightly larger than the critical size of nucleus. The appearing crystals are found to be of roughly spherical shape [41]. As we did no additional experiment on the used system (e.g., SALS), no further information of the shape of the critical nuclei is obtained.

From this time resolved observation method nucleation rates were determined from counts of newly appearing crystallites per time interval in the observed volume V_0. To determine the nucleation rate density J we need to divide by the time dependent free volume V_F. In general the relative free volume is given as $F=V_F/V_0$ which decreases from 1 to zero in the course of time due to nucleation in the bulk and subsequent growth. We assume a spatially random (Poisson) distribution of nucleation events throughout V_0 followed by growth with a constant velocity v. In a real experiment crys-

tals do not grow without limit—rather, they stop growing and hence stop reducing the free volume upon intersection with each other and/or the wall crystal. Including the overlap volume between bulk crystals for spherically growing crystallites and the overlap between wall crystal and bulk crystals leads to a simple extension of Avramis [52] and Kolmogorovs [55] result which reads

$$F(t) = \left(\frac{V_0 - 2Ad_0 - 2Avt}{V_0 - 2Ad_0}\right) \times \exp\left(-\frac{4\pi}{3}\sum_{i=1}^{j}\frac{m_i}{V_0 - 2Ad_0 - 2Av\tau_i}[R_0 + v(t-\tau_i)]^3\right), \quad (7)$$

where A is the area under investigation, d_o is the thickness of the wall crystal which may be present at $t=0$ and v is the growth velocity of both spherical bulk and wall crystals. R_0 is the finite radius of the bulk crystals at the time $t=\tau_i$, where they are large enough to be observed with the microscope. A detailed derivation of Eq. (1) is given in [41]. Using this method the time trace of the nucleation rate density is obtained. At low undercoolings the nucleation rate density is nearly constant in time, whereas a peaked nucleation rate density is observed at higher undercoolings [41].

The direct video observation results were taken at particle concentration $<21\ \mu\text{m}^{-3}$. For higher concentrations the nucleation becomes too fast to be monitored in this way. However, it is still possible to obtain an average nucleation rate density from the analysis of the average crystal size. One possibility is the use of the Avrami model. In a series of papers this author developed a model, applicable for the case of constant nucleation rate densities J and constant growth velocity v, which has since been applied to many atomic systems and also to charged colloidal suspensions where crystal growth is linear in time and the nucleation rate density is approximately constant [52,39]. The model assumes noninteracting crystallites nucleating at random positions and growing undisturbed until their volume is equal to the sample volume. The resulting crystallite density is given by the simple expression $\rho=(\alpha J/v)^{(3/4)}$, where $\alpha=0.8636$ is a geometrical factor, v is the growth velocity, and $\rho=1/V_C^3$ is the crystallite density as calculated by the average crystal volume V_C. The average steady state nucleation rate densities J_{AVR} may be calculated from v and ρ. Rewriting the above equation for ρ yields

$$J_{AVR} = 1.158v\rho^{(4/3)}. \quad (8)$$

The average linear dimension of the crystallites was measured in the mosaiclike image taken after complete solidification, and before significant ripening processes had occurred, using image processing software. Crystallites were approximated as cubes with a side length L equal to the mean of shortest and longest elongation in the 2D projection image. In this way the crystallite size distribution was obtained and the average crystal size $\langle L\rangle$ was determined. The crystallite sizing worked well for $L\geq 25\ \mu$m. For smaller L discrimination problems due to vanishing contrast between individual crystallites became significant.

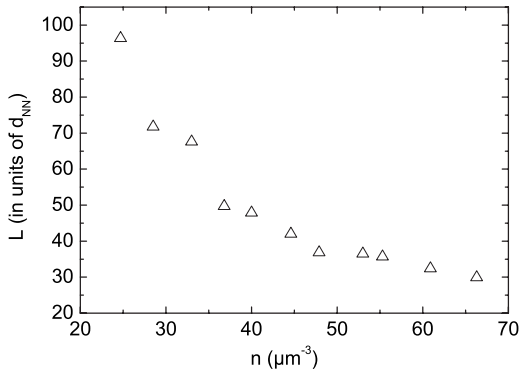

FIG. 2. Apparatus function corrected value for crystallite sizes in units of the nearest neighbor distance after complete solidification vs particle number density.

E. Static light scattering

Alternatively $\langle L\rangle$ may be determined by static light scattering. The light scattering intensity $I(q)$ (where q is the scattering vector) was recorded using the Debye-Scherrer technique on samples solidified in cylindrical flow through cells. The intensity data were taken immediately after complete solidification and before significant ripening had occurred. As determined from the appearance of a finite shear modulus [39], solidification times τ decreased from some minutes to less than a second as n was increased from the freezing point n_F to $n=66.3\ \mu\text{m}^{-3}$. Simultaneously, a pronounced broadening of the principle peak is observed due to a decrease of crystallite sizes $\langle L\rangle$. At concentrations above $n\geq 70\ \mu\text{m}^{-3}$ multiple scattering and backscattering of the sample becomes too strong to get reliable data.

A quantitative measure of $\langle L\rangle$ may be obtained from the full width at half height Δq of the Bragg-reflections as $\langle L\rangle = 2\pi K/\Delta q$, where K is the Scherrer constant of order of one [6]. At each concentration five diffraction patterns were measured and analyzed to obtain a meaningful average crystallite size $\langle L\rangle$. Unlike x-ray scattering, here the cylindrical index matching bath and sample cell act as lenses which cannot be fully corrected. In addition the detection optics, consisting of two lenses and a multimode fiber, have an influence on the broadening of the intensity peaks and therefore on the full width at half height. Therefore, great care was taken to determine the experimental resolution and record the apparatus function. A delta function would be broadened to $0.06\ \mu\text{m}^{-1}$ corresponding to 0.775°. The corrected crystallite size is shown in Fig. 2. $\langle L\rangle$ decreases continuously to values of about 30 d_{NN} at $n=66.3\ \mu\text{m}^{-3}$. This average crystallite size is used later for the calculations using the Avrami model of nucleation.

The nucleation kinetics of PnBAPS68 have been studied using video microscopy, microscopic analysis of solidified samples and by static light scattering analysis on solidified samples using either Eq. (1) or (2). The combination of the three methods allows the determination of J over 6.5 orders of magnitude as shown in Fig. 3, while n is increased only by a factor of 4. A clear bending of the curve is observed: In the low density regime the data shows a very steep increase,

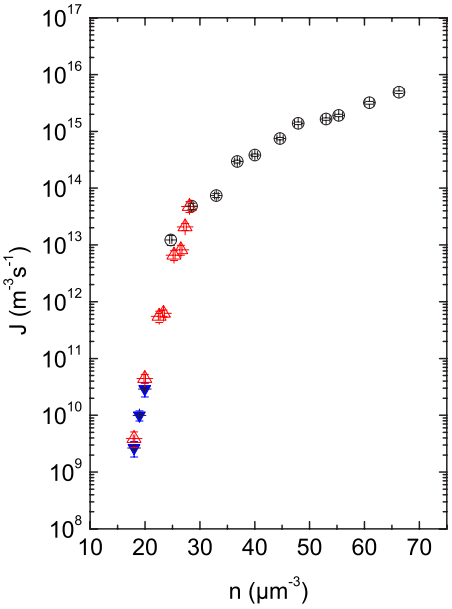

FIG. 3. (Color online) Nucleation rate densities for deionized samples of PnBAPS68 under deionized conditions. Experimental uncertainties in J are on the order of 30–70 %. Data from different experiments show quantitative agreement in the ranges of equal particle number densities. Filled triangles: J from video microscopy evaluated using Eq. (1); open triangles: J from microscopic analysis of solidified samples using Eq. (2); circles: J from light scattering data obtained from solidified samples using Eq. (2). Note the 6.5 orders of magnitude increase in J as n is increased by a factor of 4.

while for higher particle number density the increase becomes more and more flat. Each method has its own range of applicability but there is a significant overlap between them. The resulting errors in J are on the order of 30–70 % and therefore compare favorably to those usually encountered in atomic systems which often comprise one or two orders of magnitude. This accuracy is more than sufficient for comparison with classical nucleation theory, as will be performed in the following sections.

In order to be able to carry out this comparison we first have to determine the difference in the chemical potential between melt and crystal. We then demonstrate three approaches to interprete our data within the framework of CNT and continue with a critical discussion.

IV. DATA EVALUATION AND DISCUSSION

The difference in the chemical potential $\Delta\mu$ was determined from microscopic measurements of the growth velocity and subsequent evaluation of the growth data by means of the Wilson-Frenkel law (see Sec. III B). The dependence of $\Delta\mu$ on the particle number density n is nearly linear in the concentration range examined, as is shown in Fig. 4.

Therefore there are only two undefined physical values left in Eq. (4). These are the surface tension γ and the self diffusion coefficient D_S^L. Both values can in principle be functions of the particle number density. In the following data analysis we will determine the kinetic prefactor and the crystal surface tension.

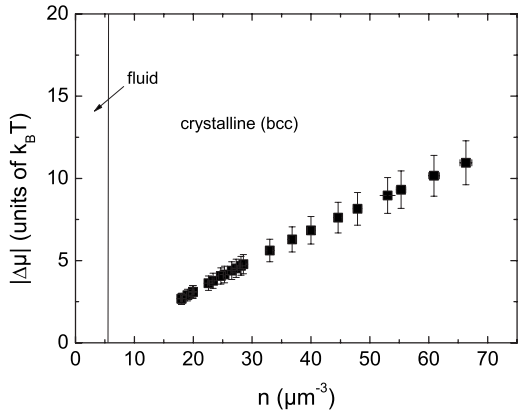

FIG. 4. Dimensionless chemical potential difference as a function of the particle number density n for the PnBAPS68 sample determined from growth measurements followed by an evaluation with the Wilson-Frenkel law. Over the investigated concentration range, $\Delta\mu$ shows a nearly linear dependence on n.

A. Method: "Graphical evaluation" of the nucleation rate density

The first method we used is a quite simple, universal, and robust one. It does not use the representation of the kinetic prefactor according to Eq. (3), and thus avoids the need of the exact knowledge of the diffusion coefficient D_S^L, surface tension, etc. For this purpose a specific logarithmic diagram, shown in Fig. 5, is used, where the nucleation rate density is plotted against $(n\Delta\mu)^{-2}$ as a measure for the inverse under-

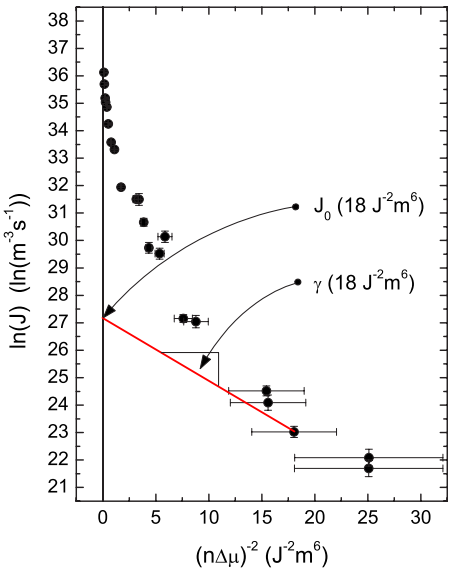

FIG. 5. (Color online) Nucleation rate densities versus $(n\Delta\mu)^{-2}$. The plot shows that with decreasing undercooling of the metastable melt (decreasing particle number density) the nucleation rate density deviates from an exponential decay. The explanation for this behavior is a concentration dependence of the surface tension of the nuclei. The red line represents the slope of the curve at $(n\Delta\mu)^{-2} = 18\ \mathrm{J}^{-2}\,\mathrm{m}^6$. The surface tension and the kinetic prefactor can be determined simply by determination of the local slope in each data point.

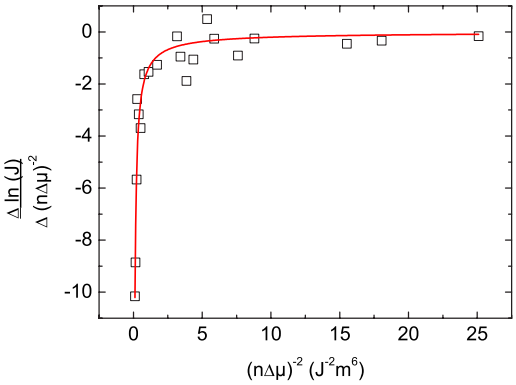

FIG. 6. (Color online) Local slope $m(n)=\Delta \ln(J)/\Delta(n\Delta\mu)^{-2}$ of the logarithmic nucleation rate density plotted versus the inverse undercooling $(n\Delta\mu)^{-2}$. The red line is a guide for the eye. Using this local slope we are able to calculate the surface tension as a function of particle number density by means of Eq. (3): $\gamma(n)=[3m(n)k_BT/16\pi]^{1/3}$.

cooling of the system. Taking the logarithm of Eq. (1) leads to

$$\ln(J) = \ln(J_0) - \frac{16\pi\gamma^3}{3k_BT}\frac{1}{(n\Delta\mu)^2}. \tag{9}$$

For a constant surface tension and a constant kinetic prefactor we would expect the data to be a straight line with the slope $m=16\pi\gamma^3/k_BT$ according to Eq. (9). Instead, the slope of the measured data is getting smaller as the undercooling is reduced. This indicates that the surface tension as well as the kinetic prefactor is a function of the particle number density: $m(n)=16\pi\gamma(n)^3/k_BT$ and $J_0(n)=1.55\times10^{11}n^{4/3}\sqrt{\gamma(n)}D_S^L(n)$.

By determining the local slope along the plot of J versus $(n\Delta\mu)^{-2}$ the surface tension as well as the prefactor can be calculated as a function of the undercooling and therefore the particle number density. The local slope is calculated using $m(n)=\Delta \ln(J)/\Delta(n\Delta\mu)^{-2}$. The result is shown in Fig. 6. The red curve is a power series curve used as a guide for the eye. The concentration dependent surface tension is then given by $\gamma(n)=(3m(n)k_BT/16\pi)^{1/3}$, which is represented as filled circles in Fig. 7. The kinetic prefactor $J_0(n)$ is defined by the intercept with the ordinate and is shown in Fig. 8.

B. Method: Fitting of nucleation rate densities

As shown above, both the surface tension and the diffusion constant are functions of n. So we are using the following expression to describe the data using a χ^2 fit:

$$J(n) = An^{4/3}\sqrt{\gamma(n)}D_S^L(n)\exp\left(-\frac{16\pi\gamma(n)^3}{3k_BT(n\Delta\mu)^2}\right), \tag{10}$$

with variable a surface tension $\gamma(n)=b_0+b_1n+b_2n^2$ and a n-dependent diffusion constant $D_S^L(n)=(a_0+a_1n+a_2n^2)D_0$, whereas a_i and b_i are the fit parameters, A is a fixed scaling parameter, and D_0 is the Stokes-Einstein diffusion coefficient $D_0=k_BT/6\pi\eta a$ (where η is the viscosity of the surrounding fluid). The fit curve shown in Fig. 8 describes the measured data quite well over the entire measured concentration regime. The surface tensions and kinetic prefactors obtained from the fit are shown in Fig. 7 and Fig. 8.

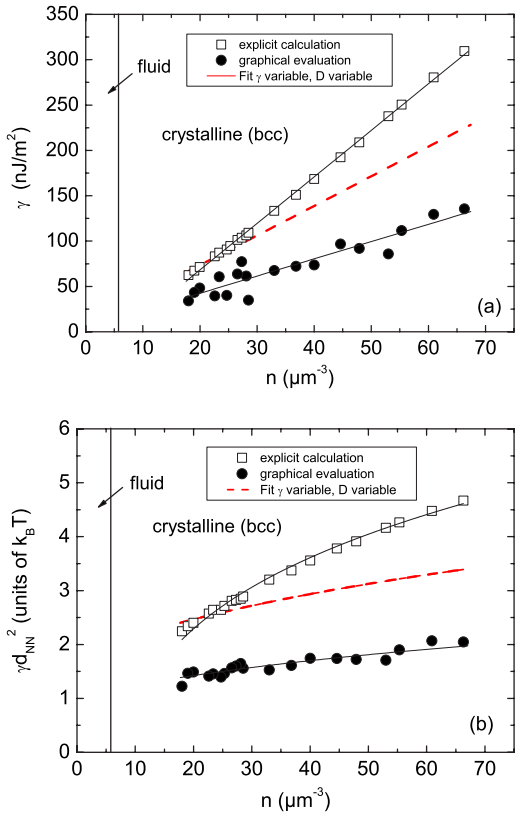

FIG. 7. (Color online) (a) Absolute and (b) reduced surface tension versus n for different evaluation methods. Open squares: Surface tension as calculated from Eq. (4). Filled circles: Surface tension as extracted by the graphical evaluation of the plot in Fig. 5. The thin black lines are linear fits to the data. The dashed red line are the values extracted from the CNT fit procedure in Fig. 8.

C. Method: Explicit calculation of the surface tension

Another possibility to analyze the data is to use the numerical expression provided by CNT [Eq. (4)] to calculate the surface tension, which requires knowing the values of D_S^L. With known diffusion coefficient it is possible to solve Eq. (4) for γ as the only remained unknown physical quantity. After obtaining γ, the prefactor J_0 can be calculated. In the following we summarize relevant results from the literature describing the long-term dynamics in charged colloidal model systems.

For charged sphere fluids D_S^L was determined experimentally by forced Rayleigh scattering and from Brownian dynamics simulation without hydrodynamic interactions and was found to be $D_S^L=0.1D_S^S$ at freezing, where D_S^S is the measured short time self diffusion coefficient [56]. Blees and co-workers did extensive measurements of the diffusion coefficient in charged colloids with 84 nm in diameter under high salt conditions (>8 mM) over a wide range of concentrations up to 15% in volume fraction. They found a linear decrease of the self-diffusion coefficient with increasing volume fraction $D_S^L=D_0(1-k\Phi)$, were Φ is the volume fraction

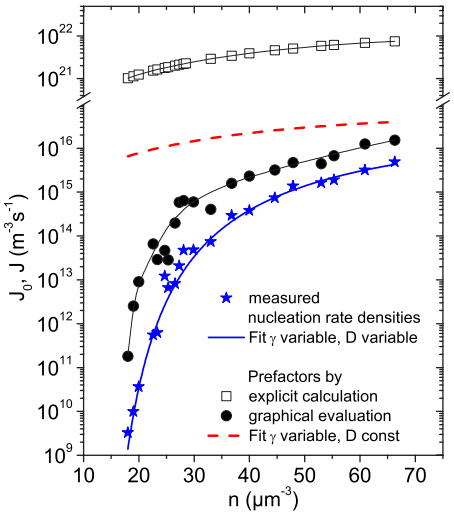

FIG. 8. (Color online) Measured nucleation rate densities and kinetic prefactors derived using the methods described in Fig. 7. The thin black lines are guides for the eye. The thick blue line is a fit to the measured data, with both surface tension and diffusion coefficient allowed to vary: $D_S^L=(a_0+a_1n+a_2n^2)D_0$ and $\gamma=b_0+b_1n+b_2n^2$.

and k a constant determined to be around 2.85 [57]. Van Blaaderen and co-workers determined the long time self-diffusion in charge spheres ($a=122$ nm) over a wide range of particle and salt concentrations. Their data can be described using constants k between 3 and 7 depending on the used salt concentration and the volume fraction regime [58]. Systematic measurements in the shearmolten melt above melting are still missing.

It is possible to obtain the n dependence of the Diffusion coefficient from the fitting procedure shown in Fig. 8 by normalizing $D_S^L(n)/D_0=(a_0+a_1n+a_2n^2)$ to 0.1 at freezing ($n_F=6.1$ μm^{-3}) using the following approximation: $D_S^S=D_0$. This simple approximation holds because the electrostatic interaction has only a very weak influence on the short time self-diffusion. In addition the volume fraction of the used samples is very low ($\Phi<1.1\%$) so that the hydrodynamic interaction can be neglected [59–62].

We obtain a nearly linear decrease with increasing particle concentration which is in good agreement with previous investigations, obtaining a value for k around 4.5. Using Eq. (4) we can now obtain a numerical solution for the surface tension. The results are shown in Fig. 7 as open squares, and the calculated prefactors are shown in Fig. 8.

V. DISCUSSION

Figure 7 shows a comparison of the determined surface tensions using the three different methods of analyzing the data. The surface tensions determined using the "graphical evaluation method" are shown by the closed circles. These data can be well described using a linear fit, despite the scatter. The reason for the scatter lies in the definition of the local slope through the calculation of the average slope between two data points and their low number. The thick dashed red line represents the surface tension stemming from the fitting procedure shown in Fig. 8. The open squares in Fig. 7 are obtained using the third method. Both datasets are showing a linear increase. Thus we can conclude from this analysis that each of the other methods agree that the surface tension is a linear function of particle number density. The surface tension increases in the case of the graphic evaluation of γ from approx. 20 nJ/m^2 to 130 nJ/m^2 (filled circles) and between 60 nJ/m^2 and 310 nJ/m^2 for the method that is based on the explicit calculation using the numerical expression provided by CNT (open squares).

For completeness the data in Fig. 7(a) is replotted as reduced surface tension, $\gamma^*=\gamma d_{NN}^2/k_BT$, in Fig. 7(b), in order to compare with atomic and molecular systems, as well to other colloidal model systems and to simulation results. Within the investigated concentration regime the measured datasets show again a linear increase on the order of a few k_BT. Note that we rescale with the nearest neighbor distance d_{NN} instead of the particle diameter $\sigma=2a$, as in charged systems particles are not closed packed. Of course the surface area taken by a particle decreases as n increases and thus d_{NN} decreases too. Of course, any increase of bulk particle density n will also increase the surface particle density proportional to $n^{2/3}$. This trivial effect is scaled out by multiplying with d_{NN}^2. Still, $\gamma^*=\gamma d_{NN}^2$ increases roughly linearly with n in all cases of our evaluation methods. This result is different to the hard sphere case where $\gamma\sigma^2$ was observed to be constant. It may, however be intuitively expected, since in our case the pair interaction energy at the nearest neighbor distance is a function of the particle number density. Loosely speaking, if the interaction increases the excess surface energy also increases. An increase of $V(d_{NN})$ is expected by the use of a Debye-Hückel potential due to the 35% decrease of d_{NN} from 343 nm to 247 nm over the investigated range of n. Closer inspection, however, reveals that the increased self screening overcompensates this effect and leads to a slight *decrease* in the pair interaction energy from $12.9k_BT$ to $12.5k_BT$. The intuitive argument thus fails in the present case. A comparison to Fig. 4 suggests instead a scaling with $\Delta\mu$, which by definition includes both the density dependence of $V(d_{NN})$ and the increasing distance from the phase boundary $n-n_F$. Possibly the relation between the thermodynamic and kinetic parameters is quite complex and our results therefore should be cross-checked with a sample where $V(d_{NN})$ increases over a similar range of experimental parameters.

As theoretical predictions for the magnitude of γ^* do not exist in the range of experimental parameters investigated here, we compare with the available experimental absolute values. Our γ^* are larger than those observed for metals, e.g., Fe with $\gamma^*\approx 0.4k_BT_M$ (with the melting temperature $T_M=1808$ K [63]) or hard spheres where $\gamma^*\approx 0.5k_BT$ [29].

Simulation results of Auer and Frenkel [22] for slightly charged hard core Yukawa particles performed for large surface potentials but strong screening ($2\kappa a=3.3-10$) should be more comparable to our results. They also observed γ^* to linearly increase from $0.24k_BT$ to $0.28k_BT$ as $\Delta\mu$ increased from 0.14 to $0.25k_BT$ (as the volume fraction is increased from 0.286 to 0.305) at a fixed surface potential of $20k_BT$ and $2\kappa a=5$. For lower surface potentials larger γ^* were ob-

served and the density dependence weakened. Fixing the surface potential to $8k_BT$ and decreasing κa from 10 to 3.3, γ^* first decreased then increased again. The values are considerably smaller then our experimental ones. A reason for this observation could be the use of different scaling factors in calculating γ^*. Auer and Frenkel used $(2a)^2$ which make sense for hard spheres, where $2a$ is close to the nearest neighbor distance d_{NN}. In our case we are scaling with d_{NN} because we are working with highly charged spheres under salt free conditions. The nearest neighbor distance is a few times larger than the particle diameter: $d_{NN} \approx (5-7) \times 2a$. Auer and Frenkel have done their simulation at a volume fraction of around 0.3 which means that $d_{NN} \approx 1.3 \times 2a$. So rescaling their γ^* values with d_{NN} does not resolve the observed discrepancy.

Figure 8 shows a comparison of the prefactors J_0 derived using the three different methods of evaluating the data. The measured nucleation rate densities are shown as blue stars. All thin lines are guides to the eye. The prefactors determined using the graphical evaluation procedure (filled circles) are about one to two orders of magnitude higher than the measured data, these two datasets have a similar shape, and are increasing about five orders of magnitude in the investigated range of particle concentration. It is obvious that the shape of the curve stemming from the fitting procedure is different to the one evaluated using the graphical method—the steep increase at low particle concentration is absent and the data are only increasing about half an order of magnitude by increasing n. At low particle number densities the data from the fitting procedure are up to five orders of magnitude larger than the data determined by graphical evaluation, only at the highest investigated particle concentration the data are close together. The open squares are showing the prefactor calculated using CNT. These prefactors are up to 10 orders of magnitude larger than those obtained by the graphical evaluation method (please notice the axis break of the ordinate) and the shape of the curve is close to the one obtained from the fitting procedure. The origin for the second observation is quite clear as we used the Diffusion coefficient obtained from the fit to calculate this dataset. But the absolute values of these prefactors are not comparable with the other ones at all.

The observation that calculated or simulated nucleation rate densities using CNT disagree with the experimental data by several orders of magnitude has been reported previously. Meyer and Stein investigated the nucleation of potassium chloride [64]. They interpreted the data by means of CNT and found deviations up to three orders of magnitude between the experiment and the numerical calculation. In addition, the slopes of the datasets are quite different. McGrawand and Laaksonen showed in a Letter that the nucleation barrier height normalized with the number of molecules in the nucleus times the free energy difference obtained by density functional calculations shows systematic departure from its classical value [65]. In a nice article Katz compares different solutions of CNT with experimental data of n-nonane: The ratio of $J_{\text{theory}}/J_{\text{experiment}}$ varies from 10^{-4} to 10^7 as a function of the undercooling and the method used for the CNT solution [66]. In a series of articles Strey and co-workers showed that CNT has to be corrected using empirical temperature correction functions to map the calculations done by CNT to the experimental data [67–70]. The deviation between CNT and experiment investigating droplet nucleation in water is about 4, in 1 pentanol 6, and in argon 35 orders of magnitude. In colloidal hard sphere systems, Auer and Frenkel did extensive simulations predicting absolute nucleation rate densities [71]. Nevertheless the simulation data are up to 15 orders of magnitude smaller than the measured nucleation rates and also the shape of the simulation data is quite different from the experiments presented in [71] and in [29].

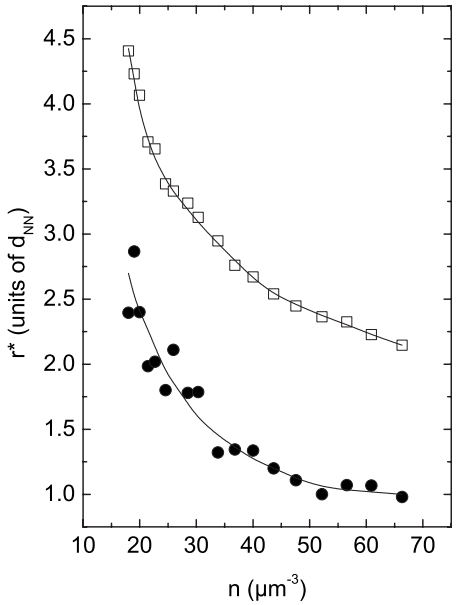

FIG. 9. Critical size of the crystal nucleus as a function of the particle concentration. Open squares: Radii as calculated by numeric resolution of Eq. (4). Filled circles: Radii as calculated using the graphical evaluation method shown in Fig. 5.

An important quantity dealing with crystal nucleation is the critical size of the crystal nucleus which is given by $r^* = -2\gamma/n\Delta\mu$. In Fig. 9 the critical radii normalized with the nearest neighbor distance calculated using the surface tensions obtained using the first method (closed symbols) and using the third method (open symbols) are plotted versus the particle number density. The thin lines are guides to the eye. The size of the critical radii decreases from approximately 4.5 down to 1 coordination shells as concentration is increased. Note that the corresponding final crystal size decreases from 100 down to 30 d_{NN} (Fig. 2). Assuming a local bcc structure of the nucleus these nuclei contain only about 500 down to 5 particles. To our knowledge there are no other experimental values published dealing with the size of the critical nucleus in highly charged colloids but our finding can be compared to measurements and simulations in other colloidal model systems and to atomic systems.

In colloidal hard spheres Elliot and co-workers found the size of a subcritical cluster at $\Phi = 0.51$ to be of about 1000 particles using video microscopy [72] and the overcritical cluster was found to be about 2500 particles close to the melting volume fraction using light scattering techniques [29]. In simulations, O'Malley and Snook determined an av-

TABLE I. Number of particles inside a critical nucleus for different systems. HS, hard sphere; CS, charge sphere; OCP, one component plasma; Expt., experimental data; Sim, from simulation; Theo, from theoretical model.

HS colloids	CS colloids	OCP	Atomic systems	Present work
>1000, Expt. [72]	150, Expt. [35]	40, Sim [75]	250–500, Sim [76]	5–500, Expt.
<2500, Expt. [29]	200, Sim [73]		150, Sim [77]	
1264, Sim [24]	50–250, Theo [74]		400, Expt. [4]	

erage size of the hard sphere nuclei at the nucleation time of 426±140 particles and 1264±480 at the induction time [24].

In weakly colloidal charged spheres Gasser and co-workers used confocal microscopy to image crystal nucleation and found critical nuclei with a radius of about 6.2 particle radii containing 150 particles [35]. Using simulations the effect of shear flow on homogeneous crystal nucleation was studied in charged colloidal systems. At lower shear rates the authors found critical nuclei of 200 particles in size [73]. Dixit and Zukoski developed an analytical model to describe crystal nucleation in colloidal charged spheres based on the basic concepts of CNT by mapping the thermodynamic properties onto an effective hard sphere system [74]. The calculated critical size of the nuclei varies between 3 and 7 effective hard sphere diameters corresponding to approximately 50 to 250 particles assuming a local bcc structure.

In a recent review, Daligault used MD simulations to study the crystal nucleation in the one component plasma [75]. Here the average number of particles per nucleus is around 40.

The kinetics of crystal nucleation in an undercooled Lennard-Jones liquid was studied using simulations by Moroni and co-workers [76]. They found that the size of the crystal nucleus strongly depends on the shape of the nucleus and its internal structure. For compact dense fcc nuclei the critical size is about 250 particles whereas 500 particles are found for clusters of nonspherical shape with a bcc/fcc structure. Numerical simulations dealing with nucleation in sodium chloride lead to a critical size of about 150 ions [77]. Experimental values for the size of the crystal nucleus in metals are tabled in the beautiful overview article written by K. F. Kelton [4]. Here the values are comparable to the ones given in the work of Moroni and co-workers. The average size of the nucleus in metals is about 400 atoms. Summarizing, we can state that the minimum size of the critical nucleus determined in our work is very small compared to other measurements or simulations as shown in Table I.

At last, we will summarize and compare the results of the important key parameters obtained by the three used evaluating methods. It was shown by using all evaluation methods that the surface tension increases linear with the undercooling. Comparing the explicit values, however, the data resulting using CNT are about a factor three larger as those of the graphical evaluation method. In addition also the kinetic prefactor using the explicit evaluation is higher: In the investigated concentration range it is several orders (up to 10) of magnitude larger than the one of the graphic evaluation. Results of the fitting procedure are always in between. Considering the critical radii another picture emerges. Here the values are unusually low for the critical nuclei according to the graphic evaluating method especially with high concentrations while the explicit calculation supplies the more realistic values compared to experimental and simulated data in various systems. We think that the origin for this discrepancy could lie with the simple picture used in CNT.

Let us remember some fundamentals concepts and assumptions of CNT concerning the appearing crystal phase and the surrounding undercooled melt. It is assumed that the crystal nucleus has only a surface tension and not a surface stress and that the shape of the nucleus is spherical. These assumptions influence the calculated barrier height in an unknown way. At the present stage we are not able to give a clear statement about the shape of the critical nucleus. Gasser *et al.* showed that the form of a critical nucleus in weak charged colloids deviates from a spherical shape [35]. Using small angle light scattering techniques He *et al.* observed deviations from a fractal dimension of three in hard sphere (HS) colloids at some volume fractions [27]. These deviations could be explained by a crystal form factor stemming from fractal highly asymmetrical objects.

In CNT the nucleation process is fundamentally described using rate equations expressing the diffusive attachment or loss of single particles to or from the crystalline nucleus. The probability that a nucleus will change its particle number is independent of its history which means that nuclei do not have any memory: there is no correlation between the attachment and the dissociation events. CNT takes also no interaction between the appearing nuclei into account. Events that nuclei collide and join together or that the particle flow to a growing nucleus influences the growth of another one are ignored. It is reported in HS colloids that this interaction between nuclei causes a drop in the number of crystals in the early stages of crystallization [29,78,79]. Surprisingly this effect is reduced by increasing the undercooling of the system. Our observation that deviations between the kinetic prefactor obtained using different ways analyzing the data is reduced by increasing the undercooling could be a hint on such a mechanism.

By describing the nucleus formation the properties of the undercooled melt are ignored too. It is assumed that the particles in the melt do not have any memory and that there are no collective modes in the melt. But density fluctuations in an undercooled melt can cause a sudden appearance of dense locally arrested regions with very slow dynamics which can lead to a crystal nucleus—rather than a stepwise growth by

single particles. This was also critically discussed by Oxtoby [80]. In a recent serious of papers van Megen and co-workers showed that the dynamics of the undercooled melt is fundamentally different to the equilibrium one [81–83]. In the equilibrium state the melt flows in the usual way while in the undercooled state it shows oriented elastic modes which could be the origin for the early stages of crystallization.

It is difficult to conceive that the simple picture used by CNT is still valid in a system with strong and long range interaction. We think that a collective assembly of particles creating a crystal nucleus could be a possible and more realistic picture. Thus a nucleus appears when particles in the first few coordination shells of the fluid rearrange to a crystal-like order. This could qualitatively explain our findings of high excess energies per particle in the interface, very small critical radii, and huge deviations in the prefactor by using the picture of single particle attachment.

VI. CONCLUSIONS

To conclude, we have measured the growth and nucleation kinetics of a charged sphere colloidal model system. Experimental nucleation data on charged spheres have been reported before. Our study, however, went beyond the mere report of decreasing crystallite sizes or solidification times. This was facilitated by the extremely narrow coexistence region of PnBAPS68 and the *in situ* control of the interaction parameters salt concentration and particle density. Only this facilitated a reliable experimental estimate of $\Delta\mu$ from growth data. In the absence of theoretical data this study presented a systematic comparison to and quantitative evaluation of measured nucleation rate densities with CNT.

One main result of our study concerns the surface tension γ which was observed to increase with particle number density, regardless of the evaluation method. The values obtained are larger than in previously investigated systems.

More detailed theoretical calculations of γ are needed to clarify the point. In particular, microscopic models of the interfacial region should be considered, as has already been done for hard spheres. In addition computer simulations including the coupling between experimental control parameters are highly warranted. Further simulations over a larger range of screening parameters and without the fixed surface potential and screening condition are highly desired. Qualitatively, however, these data are in line with the present observation in that an increase of γ^* with n was observed under nearly all conditions.

Our investigation shows another important result. It is possible to analyze the data set in a quantitative way using CNT but there are also inconsistencies observable. Using different evaluation methods leads to different results concerning the absolute values of the surface tension and its behavior as function of the particle concentration. The obtained kinetic prefactors differ up to 10 orders of magnitude and the determined minimum size of the critical nucleus is unphysically small compare to other investigations done in colloids and atomic systems. We suggest that crystal nucleation in a strongly interacting model system is much more complicated than the picture CNT proposes. A collective reassembling of particles could be a more realistic representation, and should be considered in future theoretical developments.

ACKNOWLEDGMENTS

It is a pleasure to thank T. Palberg, H. Löwen, S. Auer, and D. Frenkel as well as I. Snook, G. Bryant, and W. van Megen for stimulating discussions. Financial support by the DFG (Pa459/8 and Pa459/10) and the MWFZ, Mainz is gratefully acknowledged.

APPENDIX: DERIVATION OF THE KINETIC PREFACTOR J_0

In classical nucleation theory a spherical growing nucleus must overcome an energy barrier

$$\Delta G^* = 16\pi\gamma^3/3(n\Delta\mu)^2 \tag{A1}$$

in order to keep on growing under energy profit. Here n is the particle number density of the colloidal suspension, γ the surface tension of the crystal nucleus, and $\Delta\mu$ the chemical potential difference between the crystalline and the liquid phase. The free energy is determined by two concurrent energy terms: the surface energy $\Delta G_{\mathrm{surf}}(i)$ that must be spent in order to increase the surface of the growing nucleus, and the volume energy $\Delta G_{\mathrm{vol}}(i)$ that increases with the growing nucleus. This leads to an expression for the total energy

$$\Delta G(i) = \underbrace{4\pi\left(\frac{3}{4\pi n}\right)^{(2/3)}\gamma i^{2/3}}_{\Delta G_{\mathrm{surf}}(i)} + \underbrace{\Delta\mu i}_{\Delta G_{\mathrm{vol}}(i)} \tag{A2}$$

of a nucleus which consists of i colloidal particles.

The energy barrier ΔG^* corresponds to the critical radius $r^* = -2\gamma/n\Delta\mu$. The number of particles in a critical nucleus i^*, results from the equation

$$i^* = \frac{4}{3}\pi(r^*)^3 n = \frac{32\pi\gamma^3}{3\Delta\mu^3 n^2}. \tag{A3}$$

Cluster smaller than r^* will decay, while cluster bigger than r^* will grow because the system will decrease its energy. This simple model was first proposed by Vollmer and Weber and was extended by Becker und Döring, Zeldovich as well as Turnbull and Fisher [1–3,84]. The growth or shrinkage of the clusters is described by an attachment or separation of single particles. This process can be described using rate equations [3,4,85,86] and leads to the following result:

$$J = K^+ \cdot Z \cdot n_{\mathrm{nucleus}}. \tag{A4}$$

The steady state nucleation rate density is determined by the attachment or condensation rate K^+, describing the attachment of single particles to the crystal nucleus, by Z, the Zeldovich factor which takes the width of nucleation rate barrier into account and by the concentration of critical cluster in the melt n_{nucleus} which is described using a Boltzmann distribution:

$$n_{\text{nucleus}} = n_p^{\text{liq}} \exp(-\Delta G^*/k_B T). \tag{A5}$$

Here n_p^{liq} is the monomer concentration in the liquid, or the particle number density in the colloidal fluid.

The Zeldovich factor is connected with the second derivative of the nucleation barrier and reads as follows:

$$Z = \sqrt{\frac{(\partial^2 \Delta G/\partial i^2)_{i=i^*}}{2\pi k_B T}} = \sqrt{\frac{\Delta G^*}{3\pi k_B T i^{*2}}} = \frac{1}{8\pi} \frac{n_p^{\text{xtal}} \Delta\mu^2}{\gamma^{3/2}} \frac{1}{\sqrt{k_B T}}. \tag{A6}$$

At the critical size the evaporation rate and the condensation rate are equal and coincide with the maximum of the nucleation barrier height. But a particle attaching to the crystal nucleus has to pass the fluid crystal interface and has to cross an activation energy ΔG_A which is given by the difference in the free enthalpy between the activated cluster $\Delta G(i+1)$ and the unactivated $\Delta G(i)$. The attachment rate for a critical nucleus can therefore described using a Boltzman distribution and follows a form similar to the theory of absolute reaction rates:

$$\begin{aligned} K^+ &= 4i^{*2/3} f_0 \exp\left(\frac{-\Delta G_A}{k_B T}\right) \\ &= 4 n_p^{\text{xtal}(2/3)} \left(\frac{4\pi}{3}\right)^{2/3} \left(\frac{2\gamma}{n_p^{\text{xtal}} \Delta\mu}\right)^2 f_0 \exp\left(\frac{-\Delta G_A}{k_B T}\right). \end{aligned} \tag{A7}$$

f_0 is the vibration frequency of the particles and n_p^{xtal} is the particle number density of the crystalline nucleus. Assuming that the activation energy can be expressed using the diffusion coefficient D and the interparticle distance in the fluid d_{NN}

$$f_0 \exp\left(\frac{-\Delta G_A}{k_B T}\right) = \frac{6D}{d_{NN}^2}, \tag{A8}$$

the attachment rate K^+ reads

$$\begin{aligned} K^+ &= 24 \left(\frac{4\pi}{3}\right)^{2/3} \left(\frac{2\gamma}{n_p^{\text{xtal}} \Delta\mu}\right)^2 \frac{D}{d_{NN}^2} n_p^{\text{xtal}^{(2/3)}} \\ &= 24 \left(\frac{4\pi}{3}\right)^{2/3} \left(\frac{2\gamma}{\Delta\mu}\right)^2 D n_p^{\text{xtal}^{(-4/3)}} n_p^{\text{liq}^{(2/3)}}. \end{aligned} \tag{A9}$$

By substituting Eqs. (A9), (A6), and (A5) into Eq. (A4) one arrives at the final result for the nucleation rate density:

$$J = 12 \left(\frac{4}{3}\right)^{2/3} \pi^{-1/3} \sqrt{\frac{\gamma}{k_B T}} D n_p^{\text{xtal}^{(-1/3)}} n_p^{\text{liq}^{(5/3)}} \exp(-\Delta G^*/k_B T). \tag{A10}$$

In monodisperse charged colloidal systems under fully deionized conditions, the particle number density of the crystal and the fluid are equal and so we end up with the following simple expression:

$$J = 1.55 \times 10^{11} n^{4/3} \sqrt{\gamma} D_S^L(n) \exp\left(\frac{-16\pi\gamma^3}{3 k_B T (n\Delta\mu)^2}\right). \tag{A11}$$

[1] M. Volmer and A. Weber, Z. Phys. Chem. **119**, 227 (1926).
[2] R. Becker and W. Döring, Ann. Phys. **24**, 719 (1935).
[3] D. Turnbull and J. C. Fisher, J. Chem. Phys. **17**, 71 (1949).
[4] K. F. Kelton, Solid State Phys. **45**, 75 (1993).
[5] P. Bartlett and W. v. Megen, in *Granular Matter*, edited by A. Mehta (Springer, New York, 1994).
[6] T. Palberg, J. Phys.: Condens. Matter **11**, R323 (1999).
[7] V. J. Anderson and H. N. W. Lekkerkerker, Nature (London) **416**, 811 (2002).
[8] A. Yethiraj and A. v. Blaaderen, Nature (London) **421**, 513 (2003).
[9] S. Tang, Z. Hu, Z. Cheng, and J. Wu, Langmuir **20**, 8858 (2004).
[10] D. M. Herlach, R. F. Cochrane, I. Egry, H. J. Fecht, and A. L. Greer, Int. Mater. Rev. **38**, 273 (1993).
[11] M. Würth, J. Schwarz, F. Culis, P. Leiderer, and T. Palberg, Phys. Rev. E **52**, 6415 (1995).
[12] W. van Megen, Transp. Theory Stat. Phys. **24**, 1017 (1995).
[13] A. Heymann, A. Stipp, and K. Schätzel, Nuovo Cimento Soc. Ital. Fis., D **16D**, 1149 (1995).
[14] C. T. Lant, A. E. Smart, D. S. Cannell, W. V. Meyer, and M. P. Doherty, Appl. Opt. **36**, 7501 (1997).
[15] P. S. Francis, S. Martin, G. Bryant, W. van Megen, and P. A. Wilksch, Rev. Sci. Instrum. **73**, 3878 (2002).
[16] A. van Blaaderen, R. Ruel, and P. Wiltzius, Nature (London) **385**, 321 (1997).
[17] M. S. Elliot, M. D. Haddon, and W. C. K. Poon, J. Phys.: Condens. Matter **13**, L553 (2001).
[18] M. D. Elliot and W. C. K. Poon, Adv. Colloid Interface Sci. **92**, 133 (2001).
[19] J. S. van Duijneveldt and D. Frenkel, J. Chem. Phys. **96**, 4655 (1992).
[20] J. D. Gunton, J. Stat. Phys. **95**, 903 (1999).
[21] S. Auer and D. Frenkel, Nature (London) **409**, 1020 (2001); **413**, 711 (2001).
[22] S. Auer and D. Frenkel, J. Phys.: Condens. Matter **14**, 7667 (2002).
[23] N. M. Dixit and C. F. Zukoski, Phys. Rev. E **64**, 041604 (2001); **66**, 051602 (2001).
[24] B. O'Malley and I. Snook, Phys. Rev. Lett. **90**, 085702 (2003).
[25] A. Stipp, A. Heymann, Chr. Sinn, and T. Palberg, Prog. Colloid Polym. Sci. **118**, 266 (2001).
[26] J. L. Harland, S. I. Henderson, S. M. Underwood, and W. van Megen, Phys. Rev. Lett. **75**, 3572 (1995).
[27] Y. He, B. J. Ackerson, W. van Megen, S. M. Underwood, and K. Schätzel, Phys. Rev. E **54**, 5286 (1996).
[28] J. L. Harland and W. van Megen, Phys. Rev. E **55**, 3054 (1996).
[29] H. J. Schöpe, G. Bryant, and W. van Megen, Phys. Rev. Lett. **96**, 175701 (2006).

[30] V. C. Martelozzo, A. B. Schofield, W. C. K. Poon, and P. N. Pusey, Phys. Rev. E **66**, 021408 (2002).
[31] H. A. Wilson, Philos. Mag. **50**, 238 (1900); J. Frenkel, Phys. Z. Sowjetunion **1**, 498 (1932).
[32] D. J. W. Aastuen, N. A. Clark, L. K. Cotter, and B. J. Ackerson, Phys. Rev. Lett. **57**, 1733 (1986); **57**, 2772 (1986).
[33] M. S. Ripoll, C. F. Tejero, and M. Baus, Physica A **234**, 311 (1996).
[34] J. K. G. Dhont, C. Smits, and H. N. W. Lekkerkerker, J. Colloid Interface Sci. **152**, 386 (1992).
[35] U. Gasser, E. Weeks, A. Schofield, P. N. Pusey, and D. A. Weitz, Science **292**, 258 (2001).
[36] S. Auer, W. C. K. Poon, and D. Frenkel, Phys. Rev. E **67**, 020401(R) (2003).
[37] D. J. W. Aastuen, N. A. Clark, J. C. Swindal, and C. D. Muzny, Phase Transitions **21**, 139 (1990).
[38] M. Ishikawa and T. Okubo, J. Cryst. Growth **233**, 408 (2001).
[39] H. J. Schöpe and T. Palberg, J. Phys.: Condens. Matter **14**, 11573 (2002).
[40] P. Wette, H. J. Schöpe, J. Liu, and T. Palberg, Europhys. Lett. **64**, 124 (2003).
[41] P. Wette, H. J. Schöpe, and T. Palberg, J. Chem. Phys. **123**, 174902 (2005).
[42] W. B. Russel, Phase Transitions **21**, 127 (1990).
[43] M. Evers, N. Garbow, D. Hessinger, and T. Palberg, Phys. Rev. E **57**, 6774 (1998).
[44] P. Wette, H.-J. Schöpe, R. Biehl, and T. Palberg, J. Chem. Phys. **114**, 7556 (2001).
[45] P. Wette, H. J. Schöpe, and T. Palberg, J. Chem. Phys. **116**, 10981 (2002).
[46] P. Wette, H. J. Schöpe, and T. Palberg, Colloids Surf., A **222**, 311 (2003).
[47] J. Liu, H. J. Schöpe, and T. Palberg, Part. Part. Syst. Charact. **17**, 206 (2000); **18**, 50 (2000).
[48] M. O. Robbins, K. Kremer, and G. S. Grest, J. Chem. Phys. **88**, 3286 (1988).
[49] J. Liu, H. J. Schöpe, and T. Palberg, J. Chem. Phys. **116**, 5901 (2001).
[50] E. J. Meijer and D. Frenkel, J. Chem. Phys. **94**, 2269 (1991).
[51] M. J. Stevens and M. O. Robbins, J. Chem. Phys. **98**, 2319 (1993).
[52] M. Avrami, J. Chem. Phys. **7**, 1003 (1939); **8**, 212 (1940); **9**, 177 (1941).
[53] Y. Monovoukas, G. G. Fuller, and A. P. Gast, J. Chem. Phys. **93**, 8294 (1993).
[54] G. Pan, A. K. Sood, and S. A. Asher, J. Appl. Phys. **84**, 83 (1998).
[55] Cited by G. S. Zhadanov, in *Crystal Physics*, translated and edited by A. F. Brown (Academic, New York, 1965).
[56] F. Bitzer, T. Palberg, H. Lowen, R. Simon, and P. Leiderer, Phys. Rev. E **50**, 2821 (1994).
[57] H. Bless, J. M. Geurts, and J. C. Leyte, Langmuir **12**, 1947 (1996).
[58] A. van Blaaderen, J. Peetermans, G. Maret, and J. K. G. Dhont, J. Chem. Phys. **96**, 4591 (1992).
[59] A. van Veluwen, H. N. W. Lekkerkerker, C. G. de Kruif, and A. Vrij, J. Chem. Phys. **87**, 4873 (1987).
[60] A. P. Philipse and A. Vrij, J. Chem. Phys. **88**, 6459 (1988).
[61] R. Xu, Langmuir **14**, 2593 (1998).
[62] M. Watzlawek and G. Nägele, Phys. Rev. E **56**, 1258 (1997).
[63] A. C. Zettelmoyer, *Nucleation* (Dekker, New York, 1969), p. 279.
[64] H. J. Meyer and B. J. Stein, J. Cryst. Growth **49**, 707 (1980).
[65] R. McGraw and A. Laaksonen, Phys. Rev. Lett. **76**, 2754 (1996).
[66] J. L. Katz, Pure Appl. Chem. **64**, 1661 (1992).
[67] K. Iland *et al.*, J. Chem. Phys. **121**, 12259 (2004).
[68] J. Wölkl *et al.*, J. Chem. Phys. **117**, 4954 (2002).
[69] M. Gharibeh *et al.*, J. Chem. Phys. **122**, 094512 (2005).
[70] A. Fladerer and R. Strey, J. Chem. Phys. **124**, 164710 (2006).
[71] S. Auer and D. Frenkel, J. Chem. Phys. **120**, 3015 (2004).
[72] M. S. Elliot, S. B. Haddon, and W. C. K. Poon, J. Phys.: Condens. Matter **13**, L533 (2001).
[73] R. Blaak, S. Auer, D. Frenkel, and H. Lowen, Phys. Rev. Lett. **93**, 068303 (2004).
[74] N. M. Dixit and CH. F. Zukoski, J. Phys.: Condens. Matter **15**, 1531 (2003).
[75] J. Daligault, Phys. Rev. E **73**, 056407 (2006).
[76] D. Moroni, P. Reinten Wolde, and P. G. Bolhuis, Phys. Rev. Lett. **94**, 235703 (2005).
[77] C. Valeriani, E. Sanz, and D. Frenkel, J. Chem. Phys. **122**, 194501 (2005).
[78] Z. Cheng, P. M. Chaikin, J. Zhu, W. B. Russel, and W. V. Meyer, Phys. Rev. Lett. **88**, 015501 (2002).
[79] H. J. Schöpe, G. Bryant, and W. v. Megen (unpublished).
[80] D. W. Oxtoby, J. Phys.: Condens. Matter **4**, 7627 (1992).
[81] W. van Megen, Phys. Rev. E **73**, 020503(R) (2006).
[82] W. van Megen, T. C. Mortensen, and G. Bryant, Phys. Rev. E **72**, 031402 (2005).
[83] S. R. Williams, P. McGlynn, G. Bryant, I. K. Snook, and W. van Megen, Phys. Rev. E **74**, 031204 (2006).
[84] J. Zeldovich, J. Exp. Theor. Phys. **12**, 525 (1942).
[85] F. C. Collins, Z. Elektrochem. **59**, 404 (1955).
[86] B. Mutaftschiev, in *Handbook of Crystal Growth*, edited by D. T. J. Hurle (Elsevier, Amsterdam, 1993), Vol. 1.